Thermal, Spectroscopy, and Mechanical Properties of Biodegradable Polymers and Reinforcements: A Green Approach

João J. Melo dos Santos , Evanimek B. Sabino da * , Carlos A. Paskocimasa

Posted Date: 17 November 2023

doi: 10.20944/preprints202311.1154.v1

Keywords: Nanocellulose; Biodegradability; Sustainability; Additive manufacturing; Functional materials.

Research paper

Thermal, Spectroscopy, and Mechanical Properties of Biodegradable Polymers and Reinforcements: A Green Approach

João J. Melo dos Santos [1], Evanimek B. Sabino da Silva [2,*] and Carlos A. Paskocimas [1]

[1] a Programa de ciências e engenharia dos materiais, Universidade Federal do Rio Grande do Norte, Natal, RN, Brazil

[2] - Instituto de Química, Universidade Federal do Rio Grande do Norte, Natal, RN, Brazil.

* Correspondence: evanimek.sabinodasilva@usach.cl Tel: +55 (84) 99841-0503

Abstract: Biocomposite membranes based on polylactic acid (PLA) and cellulose nanocrystals (CNCs) were developed using a scientific approach. Dicumyl peroxide (DCP) was used as a polymerization initiator, while tin octoate ($Sn(Oct)_2$) and triphenylphosphane ($P(C_6H_5)_3$) were used as catalysts. A torque rheometer was used to mix the components of the biocomposite, and thin films was prepared by solvent casting. Fourier transform infrared (FTIR) spectroscopy confirmed the coupling between the PLA and CNCs. Field emission scanning electron microscopy (FESEM) showed that the CNCs were well-dispersed in the PLA matrix with an unimodal particle size distribution and a maximum particle size of around 200 nm. Thermogravimetric analysis (TGA) and differential scanning calorimetry (DSC) analysis demonstrated good thermal stability and improved biodegradability of the biocomposite membrane compared to pure PLA. Mechanical characterization showed a Young's modulus of 1.65 GPa, which is comparable to that of other composite materials, and a maximum tensile strength of 20.31 MPa, which is higher than that of pure PLA. These results suggest that the developed biocomposite membrane has potential applications in water filtration, food packaging, and biomedical devices.

Keywords: nanocellulose; biodegradability; sustainability; additive manufacturing; functional materials

1. Introduction

Polymer science is an area of research that has been gaining interest in recent years, particularly in the production of green materials [1]. One emerging processing technique that has shown promise is reactive extrusion, which can be used to produce biodegradable polymeric composite pellets [2]. This approach is considered a green chemistry route because it involves designing safer chemicals, using renewable feedstocks, reducing derivatives, and catalysis [3,4]. Recent studies have shown that the combination of processing and compositional parameters can improve the properties of biocomposites [5,6].

Tech has created a new kind of polymer membrane for separating crude oil into useful components [7]. The membrane could greatly reduce the energy necessary for those initial separations. They've also created artificial intelligence tools to predict the performance of these kinds of polymer membranes, which could accelerate the development of new ones. Overall, the field of polymer science is constantly evolving, with new research and developments emerging all the time [8,9].

production has been an area of research that has been gaining interest in recent years, particularly in the production of green materials [3,10]. One approach that has shown promise is the addition of natural biodegradable nanofillers, such as nanoclay or a nanocrystal of cellulose (CNC), which seems to be an improvement approach development [11,12]. By controlling the geometric dimensions, the polymer nanocharger interactions, and the incorporation of a small number of

 doi:10.20944/preprints202311.1154.v1

nanoparticles (usually less than 10% by weight), the properties of the material can be changed, such as improving mechanical strength and thermal resistance [13,14].

Recent studies have shown that the combination of processing and compositional parameters can improve the properties of biocomposites [15,16]. For example, researchers have investigated the use of Dicumyl peroxide (DCP) and lactic acid (LA) associated with tin octoate/triphenylphosphine (($Sn(Oct)_2$)/($P(C_6H_5)_3$)) to incorporate into PLA/CNC compounding by reactive extrusion, forming a polymer condensation in a PLA-g-CNC interfacial adhesion of components [4,17]. This approach has shown promise in improving the mechanical properties and conferring a biodegradable biopolymer characteristic [18,19].

Together, a group of biodegradable polymers, PLA has stood out for its low cost of production, making it one of the main candidates to substitute oil-based synthetic polymers [20]. Biodegradability, low density, low cost of production, and a reactive surface are some of the characteristics of these materials [15,21,22]. Also, these nanocrystals originate from renewable and abundant sources, such as vegetables (e.g., wood, cotton, bacterial cellulose) and animals (e.g., tunicates) [13,14].

An important characteristic of CNC is its reinforcement for the PLA matrix [23]. However, these reinforcements are commonly hydrophilic and tend to agglomerate by Vander Walls interaction during the drying process, which hinders the thermal and mechanical properties of the nanocomposites [8,24]. Therefore, the surface interaction of hydrophobic matrices in PLA-g-CNC nanocomposites must be improved [12,25].

Present research work has investigated the use of DCP and LA associated with tin ($Sn(Oct)_2$)/($P(C_6H_5)_3$) to incorporate into PLA/CNC compounding by reactive extrusion, forming a polymer condensation in a PLA-g-CNC interfacial adhesion of components [26,27].

Biopolymers are a promising alternative to oil-based synthetic polymers because they are biodegradable and renewable [28]. One of the most important biopolymers is PLA, a semi-crystalline polymer with excellent physical, chemical, and mechanical properties [29]. PLA is also versatile and can be processed using a variety of methods, including extrusion, injection molding, and torque rheometry [30].

Due to its low cost of production and good processability, PLA is a leading candidate for replacing oil-based synthetic polymers in a wide range of applications, including packaging, food service, and textiles [31]. For example, PLA can be used to make biodegradable food containers, disposable utensils, and shopping bags. It can also be used to produce biodegradable medical implants and agricultural mulch films [26,32]. PLA is a sustainable and versatile material with the potential to reduce our reliance on oil-based plastics [27].

In conclusion, CNCs are a promising nanomaterial for reinforcing PLA matrices. CNCs are biodegradable, have a low density and cost of production, and have a reactive surface. However, CNCs are hydrophilic and tend to agglomerate, which can hinder the thermal and mechanical properties of the nanocomposites [33,34]. One way to improve the interfacial adhesion between PLA and CNCs is to use reactive extrusion. In reactive extrusion, a polymerization initiator, such as DCP, and a catalyst, such as ($Sn(Oct)_2$)/($P(C_6H_5)_3$), are added to the PLA/CNC mixture. This initiates a condensation reaction between the PLA and CNCs, forming a more stable and homogeneous nanocomposite.

2. Experimental

2.1. Chemical reagents

PLA 4043D was provided by INGEO. Cyclohexane and methanol (VETEC), dicumyl peroxide (DCP 99-RETILOX), lactic acid (SYNTH), tin(II) 2-ethyl hexanoate ($Sn(Oct)_2$), and triphenylphosphine (($P(C_6H_5)_3$) from SIGMA ALDRICH were used. Cyclohexane (C_6H_{12}), methanol (CH_3OH), chloroform ($CHCl_3$), and sulfuric acid (H_2SO_4) were used to pre-wash the cotton fibers. Dicumyl peroxide ($C_{18}H_{22}O_2$) and lactic acid ($C_3H_6O_3$) were used as a radical initiator and crosslinking agent,

 doi:10.20944/preprints202311.1154.v1

respectively. Octoatetriphenylphosphine ($Sn(Oct)_2$) was applied as a reaction catalyst and a coupling agent in polymerization.

2.2. CNC preparation

Cotton fibers were dried and then introduced into a 64 wt.% solution of H_2SO_4 and CNC, following a procedure outlined in previous literature. The reaction was halted by a rapid decrease in temperature. Subsequently, the solution underwent centrifugation at 6000 rpm for 20 minutes. The CNC-containing solution was dialyzed against running water until it reached a neutral pH. Finally, the suspension was subjected to freeze-drying to yield dry CNC.

2.3. Nanocomposite manufacturing

PLA composites (Table 1) were processed using a Haake internal mixing rheometer with a mixing chamber capacity of 69 cm^3, equipped with roller-type rotors, operating at 60 rpm and 180 °C. CNC (2 wt.%) was added along with DCP (1 PHR relative to PLA content). The samples were prepared with three different percentages of LA (0.5, 1.0, and 2.0 wt.%). Equimolar amounts of $Sn(Oct)_2$ relative to LA content were also added without any organic solvent. Samples were dissolved in $CHCl_3$ at 40 °C for 2 h; after this period, the solvent was allowed to evaporate. Subsequently, nanocomposite solutions were applied to a Teflon disc (9 cm diameter) for solvent evaporation at room temperature. Tensile samples were then manufactured with dimensions of (7 x 1.5) mm, following ASTM D 882-18.

Table 1. – Literature formulations standard PLA, and composites with CNC prepared by reactive extrusion methodologies.

	ID	Sample	PLA (%)	LA (%)	CNC (%)	DCP (%)	P(C6H5)3 (%)	Sn(Oct)2 (%)	Ref.
0	P	PLA	100						[4,16]
1	PC	PLA+CNC	98		2.00				[4,35]
2	PD	PLA+DCP	99.01			0.99			[35,36]
3	PAL1_0.0045	PLA+AL1	98.99	1.00			0.0045	0.0045	[37,38]
4	PAL2_0.009	PLA+AL2	97.98	2.00			0.0090	0.0090	[37,38]
5	PAL0.5_0.0023	PLA+AL0.5	99.5	0.50			0.0023	0.0023	[37,38]
6	PDAL1_0.0045	PLA+DCP+AL1	98.01	1.00		0.98	0.0045	0.0045	[4,37]
7	PDAL2_0.009	PLA+DCP+AL2	97.01	2.00		0.97	0.0090	0.0090	[4,37]
8	PDAL0.5_0.0023	PLA+DCP+AL0.5	98.51	0.50		0.99	0.0023	0.0023	[4,37]

 doi:10.20944/preprints202311.1154.v1

9	PCD	PLA+CNC+DCP	97.03		2.00	0.97			[35,36]
10	PCAL1_0.0045	PLA+CNC+AL1	96.99	1.00	2.00		0.0045	0.0045	[38]
11	PCAL2_0.009	PLA+CNC+AL2	95.98	2.00	2.00	0.96	0.0090	0.0090	[38]
12	PCAL0.5_0.0023	PLA+CNC+AL0.5	97.5	0.50	2.00	0.95	0.0023	0.0023	[38]
13	PCDAL1_0.0045	PLA+CNC+DCP+AL1	96.03	1.00	2.00	0.97	0.0045	0.0045	[35,36]
14	PCDAL2_0.009	PLA+CNC+DCP+AL2	95.03	2.00	2.00		0.0090	0.0090	[35,36]
15	PCDAL0.5_0.0023	PLA+CNC+DCP+AL0.5	96.53	0.50	2.00		0.0023	0.0023	[35,36]

2.4. Characterization

Fracture surfaces of the samples were analyzed using a Field Emission Gun – Scanning Electron Microscope (FESEM) – CARL ZEISS Auriga, operating at 3.0 kV with a tungsten filament. Initially, all samples underwent a coating process with a thin layer of gold for 60 seconds using a Sputter Coater BAL-TEC SCD 005 within an argon atmosphere vacuum. Following this, the cryogenically fractured samples were thoroughly examined.

To investigate the chemical modification groups of the samples, Fourier Transform Infrared (FTIR) spectroscopy was employed, utilizing a Spectrum 65 spectrometer from Perkin Elmer. The analysis was conducted in attenuated total reflection (ATR) mode, employing a ZnSe crystal and scanning over the frequency range of 4000 cm^{-1} to 700 cm^{-1} with a resolution of 4 cm^{-1} and 128 scans per sample.

Thermogravimetric analyses of the samples were carried out using a Perkin Elmer STA 6000 apparatus. This aimed to evaluate the impact of coupling agents on the thermal degradation of the material. The scans were performed over a temperature range of 30 to 550 °C under a Nitrogen flow rate (99.5% purity) of 50 $ml.min^{-1}$ and with a heating rate of 10 $°C.min^{-1}$.

Differential scanning calorimetry (DSC) analyses were conducted using the TA Instruments Q600 equipment, with samples heated from 10 to 190 °C with inverse recruitment. The analyses were performed under a nitrogen atmosphere at a flow rate of 50 $mL.min^{-1}$, also with a heating increment of 10 $°C.min^{-1}$.

Evaluation of the mechanical properties, including any gain in mechanical resistance in the samples compared to pure PLA, involved conducting tensile composite tests. These tests were carried out using a universal testing machine (AG-X, Shimadzu) equipped with a load cell of 22 N, following the general recommendations of ASTM D882-18. The sample dimensions were standardized at 7 x 10 mm, and five samples were selected for resistance testing.

A comprehensive investigation into the chemical structure of the compounds, nuclear magnetic resonance of 1H NMR was employed. The spectra were recorded in $CDCl_3$ at 400 and 100 MHz using

 doi:10.20944/preprints202311.1154.v1

a Bruker instrument located in Billerica, MA, USA. The chemical shift (δ) was expressed in ppm, and the coupling constant (J) in Hz.

3. Result and discursion

3.1. Composite processing

The mechanism of grafting CNC onto PLA (PLA-g-CNC) relies on reactive extrusion through the chemistry of ring-opening polymerization (ROP). In this process, L-lactide is grafted onto a PLA molecule, initiated by a catalyst system involving $Sn(Oct)_2$. Additionally, the introduction of DCP facilitates decomposition, generating free radicals that readily react with hydroxyl groups during the PLA and CNC grafting mechanism. Furthermore, LA is associated with the dimer ring-opening of $Sn(Oct)_2$, and the resulting free hydroxyl radicals act as protective agents for the polymer matrix, as reported by Kalia et al. (2011).

Catalyst systems and the activation of free radicals act as coupling and dimerization agents. The release of free radicals from DCP, coupled with LA associated with the catalyst system, establishes a balanced equilibrium influencing the propagation rate and polymer degradation of PLA. The grafting process was carried out at a rotational speed of 60 rpm and a working temperature of 180 °C.

The grafting mechanism was meticulously assessed through FTIR analysis, as illustrated in Figure 1. Dhar et al. established a crucial vibration coupling moment between PLA and CNC polymers, as exemplified by the σ vibration band at 3333 cm^{-1}. This band signifies the stretching of the unsaturated carbon skeleton construction of CNC (-C-C-) and the presence of hydroxyl groups (-OH) [16]. This correlation is extrapolated into the ion interaction between PLA-g-CNC, indicating a chemistry affinity achieved through reactive extrusion (Figure 2c and 2d).

The effective grafting process, as discovered by Jacobsen et al. and Dhar et al., involves the ring-opening polymerization (ROP) of L-lactide, initiated from available hydroxyl groups onto the CNC surface. The equimolar composition of the catalyst system and the inclusion of DCP as coupling agents significantly contribute to this reaction [25,39]

FTIR results suggest the presence of a grafting polymer complement, indicating effective interactions between chain segments and functional groups of PLA and CNC during the polymer condensation process. This is illustrated in Figure 1a and 1c, where band minimization is demonstrated as a result of incorporating PCAL in an equimolar composition (Figure 1b and 1d).

Furthermore, Figure 1b and 1c display a reduction in the vibrational stretch band corresponding to -OH, suggesting the exclusion of this molecule from the process, confirming and maximizing the hydroxyl molar ratio.

Preprints (www.preprints.org) | NOT PEER-REVIEWED | Posted: 17 November 2023 doi:10.20944/preprints202311.1154.v1

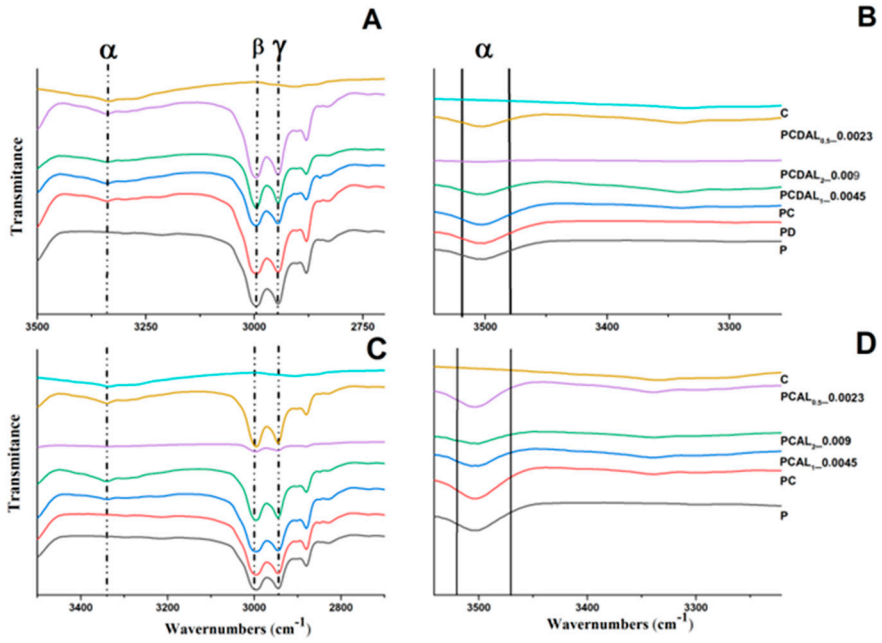

Figure 1. – FTIR spectra: (a) and (c) Illustrate the vibrational moments in the molecular composition, highlighting the hydroxyl (σ), sigma bridge in composite formation (β), and pi (π) bridge in carbonyl formation (γ) in the PC. PCAL1_0.0045, PCAL2_0.009, and PCAL0.5_0.0023 compositions. (b) and (d) Depict the relationship between the removal of hydroxyl groups and the incorporation of PLA in CNC.

Resonance magnetic hydrogen analysis (1H NMR) of the PLA and PLA-g-CNC samples, as depicted in Figure 2 (a) and 2 (b), respectively, serves to illustrate the efficiency of the grafting process. It is noteworthy that new peaks emerge at 3.68 ppm and within the range of 4.1 to 4.5 ppm. The newly observed peak at 3.68 ppm corresponds to the protons of the methyl group formed in the PLA-g-CNC structure. The presence of these protons has been previously reported in the work of Dhar et al., where a combination of PLA and CNC was also employed [15,16,40].

The peaks within the range of 4.2 and 4.4 ppm correspond to the methylene protons in the cellulose structure, providing conclusive evidence of the presence of CNC in the grafted structure010; Dufresne 2017). In the 1H NMR spectra of pure PLA (Figure 2 (a)), the peak at 3.68 ppm was not identified, and the peak at 1.5 ppm, representing the -CH_3 protons, exhibited significant changes compared to the 1H NMR spectra of PLA-g-CNC. The 1H NMR results align with those obtained by FTIR, as the -CH_3 band was observed close to 2900 cm^{-1}.

Preprints (www.preprints.org) | NOT PEER-REVIEWED | Posted: 17 November 2023 doi:10.20944/preprints202311.1154.v1

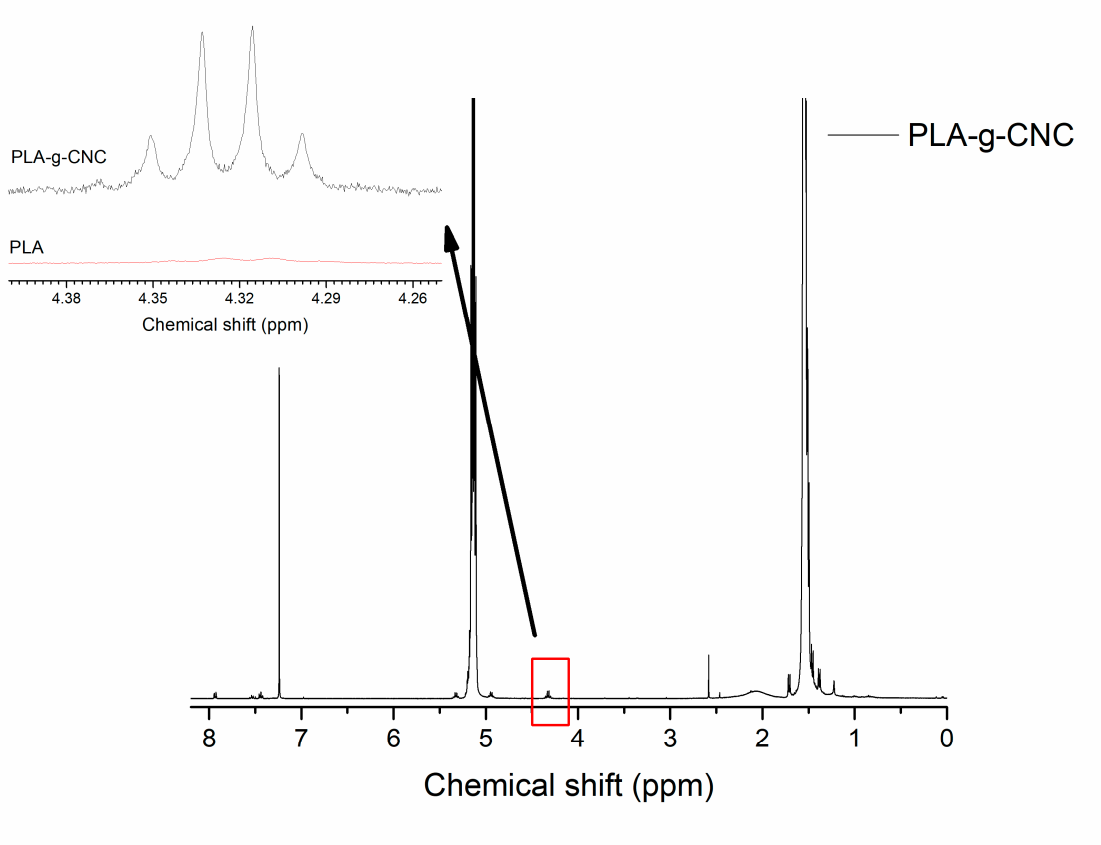

Figure 2. 1H NMR spectra of the PLA-g-CNC sample, with a focused view on the selected region (4.40 to 4.25 ppm), magnified and presented as an inset.

3.2. Field emission scanning electron microscopy (FESEM)

The morphology of CNC is illustrated in Figure 3. The CNC suspension underwent dilution and sonication before freeze-drying. The cellulose distribution exhibited excellent dispersion with a Gaussian profile. Nanocrystal cellulose displayed a monomodal distribution, with nanometric dispersion ranging from ≈ 5 to ≈ 400 nm. Notably, the maximum dispersion was observed at ≈ 200 nm, as demonstrated in Figure 3f and 3g. The needle-like structure of CNC, resulting from acid hydrolysis (H_2SO_4), revealed a whisker-like geometry. The measurement of CNC was conducted through FESEM analysis and sequential image analysis, involving the counting of approximately 400 particles using image analysis software, ImageJ. The results indicated an average diameter of ≈ 11.38 nm and a length of ≈ 237.89 nm, as shown in Figure 3a.

Preprints (www.preprints.org) | NOT PEER-REVIEWED | Posted: 17 November 2023 doi:10.20944/preprints202311.1154.v1

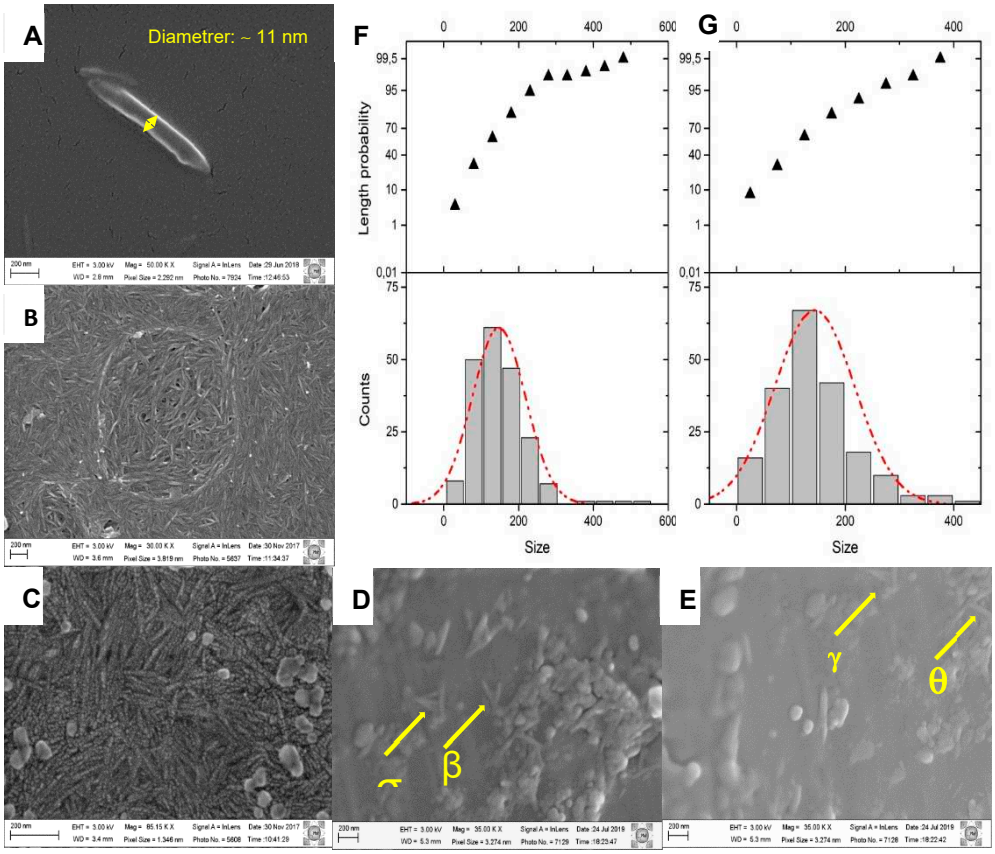

Figure 3. - Micrograph of nanofiber cellulose and nanocrystals resembling whiskers: (a) Zoomed-in image of nanofiber materials revealing a diameter of approximately 11 nm and a length of about 240 nm; (b) and (c) Micrographs of nanofibers; (d) and (e) Microscopy images showing the cryogenic fracturing surface of PLA-g-CNC samples; (f) and (g) Statistical distribution depicting a monomodal distribution of nanocrystal cellulose whiskers.

The cellulose nanocrystals used in this study had approximate dimensions of ≈ 40 nm in diameter and ≈ 200 nm in length, as shown in Figures 3d and 3e. The distribution of CNCs throughout the PLA matrix was mostly random, although some areas of higher concentration agglomeration and a diffuse crystal dispersion were observed in micrographs 3e in make γ and θ.

The effect of matrix concentration has an interaction with Vander Waals force, forcing a zone ramification. To prevent agglomeration of CNCs in the PLA matrix and maintain the transparency of the films obtained, researchers used a dilution in dialysis membrane with a continuous flow of water to obtain the neutralized material, followed by probe sonication before freeze-drying, together with associate coupling agent.

CNCs are commonly hydrophilic and tend to agglomerate by Vander Walls interaction during the drying process, which hinders the thermal and mechanical properties of the nanocomposites. To address this issue, researchers investigated the use of DCP and LA associated with $t(Sn(Oct)_2)/(P(C_6H_5)_3)$ to incorporate into PLA/CNC compounding by reactive extrusion, forming a polymer condensation in a PLA-g-CNC interfacial adhesion of components.

Biopolymers, such as semi-crystalline PLA, have shown better physical, chemical, and mechanical properties and are suitable for variable melting processing routes by extrusion methodology, injection molding, and/or torque rheometer. PLA is one of the main candidates to substitute oil-based synthetic polymers due to its low cost of production and biodegradability, low density, low cost of production, and reactive surface.

These nanocrystals originate from renewable and abundant sources, such as vegetables (e.g. wood, cotton, bacterial cellulose) and animals (e.g. tunicates). An important characteristic of CNC is

Preprints (www.preprints.org) | NOT PEER-REVIEWED | Posted: 17 November 2023 doi:10.20944/preprints202311.1154.v1

its reinforcement for the PLA matrix. However, the hydrophobic matrix surface interaction of PLA-g-CNC nanocomposites must be improved to enhance these properties.

The addition of natural biodegradable nanofillers, such as CNC, has been shown to improve mechanical properties and confer a biodegradable biopolymer characteristic. Controlling the geometric dimensions, the polymer nano-charger interactions, and incorporating a small number of nanoparticles (usually less than 10% by weight) can change the properties of the material, such as improving mechanical strength and thermal resistance.

Biopolymers, such as PLA, have been used as a suitable and promising alternative to oil-based synthetic polymers due to their low cost of production, biodegradability, low density, and reactive surface. PLA has stood out for its physical, chemical, and mechanical properties, making it one of the main candidates to substitute oil-based synthetic polymers. However, the difficulty of dispersing CNC in the PLA matrix has been reported by other researchers.

CNCs are commonly hydrophilic and tend to agglomerate by Vander Walls interaction during the drying process, which hinders the thermal and mechanical properties of the nanocomposites. To address this issue, researchers have investigated the use of DCP and LA associated with $(Sn(Oct)_2)/(P(C_6H_5)_3)$ to incorporate into PLA/CNC compounding by reactive extrusion, forming a polymer condensation in a PLA-g-CNC interfacial adhesion of components.

The improved dispersion and compatibility of the CNC nanocrystals with PLA have resulted in improved mechanical properties, such as Young's modulus and tensile strength.

3.3. Thermogravimetric analysis (TGA)

Thermogravimetric (TG) curves of neat PLA and biopolymer nanocomposites are shown in Figure 4. The addition of coupling agents (DCP, LA, and $Sn(Oct)_2/P(C_6H_5)_3$) modified the arrangement of the curves. The TG curves of samples with CNC also showed a modified profile. The derivative thermogravimetric (DTG) curves revealed a modification in the degradation parameters, indicating a change in the mass composition, possibly due to an increase in the biopolymer mass and a slower mass loss rate at higher heating temperatures. This suggests an increase in the force of interaction between the polymerized molecules.

The polymerization system consists of a chain conjugation that converts a pi (π) bond to a sigma (σ) bond, as shown in Figure 2. This coupling also increases the molecular mass and hydrogen bonding interactions. The weight loss stages of the composites, shown in Figure 4, were identified as a loss of macromolecular mass and a slow and steady event, which is attributed to the strong interaction between the formed products.

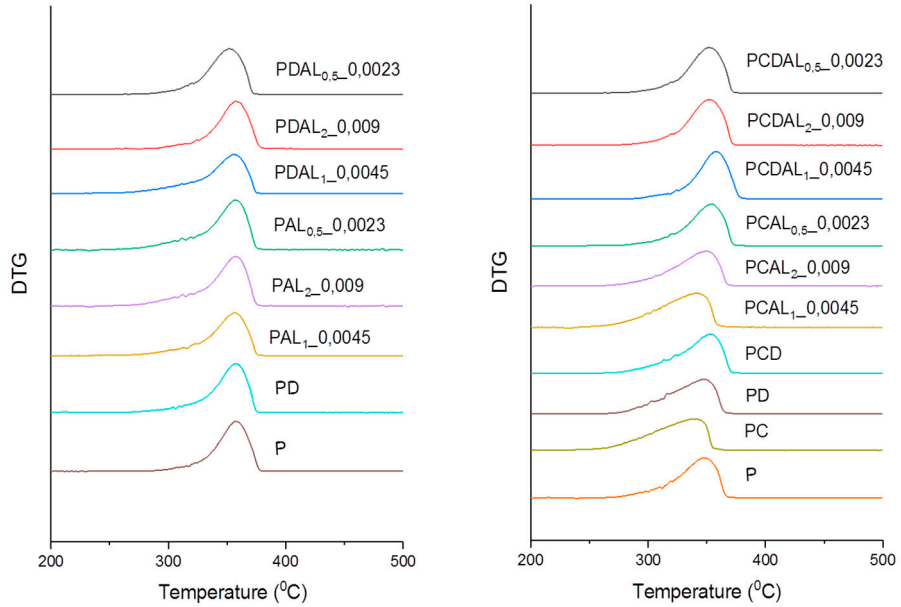

 doi:10.20944/preprints202311.1154.v1

Figure 4. – Comparative DTG analysis of neat PLA (a) and PLA-g-CNC composites (b).

The thermogravimetry results shown in Figure 4 suggest a slight improvement in thermal stability in the presence of CNC and DCP (PD and PC). This is due to polymeric propagation, which is confirmed by the possible polymer incorporation shown in Table 2. Improvements in thermal stability are obtained when C=C and C-C bonds are formed between PLA and CNC. The mechanism of ring-opening polymerization (ROP) is well-documented in the literature.

As shown in Figure 1, the vibrating moments β and γ have a minimized band frequency around 3010 cm^{-1} and 3090 cm^{-1}, respectively. This suggests that the present process activates the polymer system in two phases: electrophilic substitution and chain propagation, as observed during extrusion.

Activation energy is the minimum energy required to initiate a reaction mechanism. Dicumyl peroxide (DCP) is a crosslinking agent that forms radical molecules and induces an induction period (Salmieri et al., 2014; Dhar et al., 2016b; Kargarzadeh et al., 2017).

A multifunctional radical crosslinked with coupling agent LA (0.5 wt.% and 1 wt.%) and $(Sn(Oct)_2)/P(C_6H_5)_3$ was used to generate a high molecular weight polymer through an extrusion reactive process. This polymer showed an increased degradation temperature and mass incorporation ratio.

Table 2. Thermal measurement properties composite and weight (Wt) incorporation polymer of neat PLA and composites.

ID		ΔHm (J/g)	Xc (%)	ONSET		Maximum temperature pick degradation (0C) (PMD)	
				T (0C)	Wt%	T1/2	Wt%
0	P	21.43	23.02	319	93	353	29
1	PC	19.68	21.52	326	93	354	26
2	PD	5.52	5.99	336	93	360	29
3	PAL1_0.0045	30.74	33.35	327	94	360	20
4	PAL2_0.009	29.46	32.30	328	95	358	17
5	PAL0.5_0.0023	29.21	31.54	331	95	357	19
6	PDAL1_0.0045	23.55	25.81	329	94	358	26
7	PDAL2_0.009	30.20	33.44	331	93	359	22
8	PDAL0.5_0.0023	24.79	27.03	336	94	360	28
9	PCD	22.56	24.97	327	94	356	28
10	PCAL1_0.0045	28.32	31.37	315	94	351	25
11	PCAL2_0.009	28.78	32.22	302	94	344	16
12	PCAL0.5_0.0023	28.23	31.10	321	93	353	25
13	PCDAL1_0.0045	28.01	31.66	312	95	348	25

 doi:10.20944/preprints202311.1154.v1

14	PCDAL2_0.009	26.14	29.55	296	95	342	17
15	PCDAL0.5_0.0023	26.53	29.52	319	95	349	26

3.4. Differential scanning calorimetry (DSC)

Results from the differential scanning calorimetry (DSC) analysis of all samples are presented and shown in Table 3. The glass transition temperature (Tg) was determined to assess the dimensional stability of the polymer and nanocomposites and is revealed in Figures 5a and 5b, located in the region denoted by σ, ranging approximately between 40 to 60 °C.

PLA is a semi-crystalline polymer conducted, a study on the structural properties of nanocrystalline cellulose, focusing on the uniform distribution of methyl groups in the alpha carbon (-CH_3) through reactive extrusion in their research system. This methyl group is a representative part of the cellulose backbone, and the peptidic bond represents lateral groups in PLA-g-CNC, as observed in a melting peak.

A modest reduction in the melting temperature (Tm) of certain compositions, when compared to neat PLA (as indicated in Table 3), was observed in the temperature range of approximately 145 to 153 °C. This observation was determined at positions β and γ, revealing two consecutive temperature transitions, as depicted in Figures 5a and 5b. The decrease in crystalline domains can lead to the appearance of peaks at different temperatures.

The presence of double peaks (denoted as peaks β and γ) suggests the coexistence of two crystalline structures with a minimal difference in enthalpy transition. This phenomenon is observed through a displacement in the transition phase, where the α-crystal occurs at a temperature of approximately 148 °C, and the α'-crystal at a temperature of about 152 °C. The α-crystals exhibit a higher level of organizational crystalline structure, along with a higher fusion temperature compared to the α'-crystals, as illustrated in Figure 5a. This testing process at elevated temperatures requires an extended period for the atomic organization and rearrangement of crystalline structures from a solid state to a liquid interface.

This aligns with the degradation temperature presented in Table 2. The most favorable growth patterns of α-crystals were observed in samples where double peaks were absent, and the melting temperature (Tm) ranged from 148 to 152 ºC, excluding PDAL1_0.0045, PDAL0.5_0.0023, and PCDAL0.5_0.0023. by Jonoobi M. et al., the introduction of LA to the system resulted in the emergence of double Tm peaks, indicating that the interaction of these components contributed to a reduction in the content of α-crystals.

Furthermore, both LA and CNC, despite the addition of DCP, elevated the crystallization temperature (Tc) of neat PLA. This enhancement can be attributed to the improved mobility of ungrafted chains, surpassing the activation energy required for crystal formation.

Table 3. - DSC results (Tm, TC, Tg, and XC) of neat PLA and composites.

	ID	Tm (oC)		Tc (oC)	Tg (oC)	Xc (%)
		Tm1 (oC)	Tm2 (oC)			
0	P	152	-	113	59	23.02
1	PC	151	-	128	58.8	21.52
2	PD	148	-	141	58.6	5.99
3	PAL1_0.0045	144	150	119	55.3	33.35
4	PAL2_0.009	140	147	117	56.7	32.30

Preprints (www.preprints.org) | NOT PEER-REVIEWED | Posted: 17 November 2023 doi:10.20944/preprints202311.1154.v1

5	PAL0.5_0.0023	148	151	127	57	31.54
6	PDAL1_0.0045	149	-	128	57.8	25.81
7	PDAL2_0.009	146	150	129	56.5	33.44
8	PDAL0.5_0.0023	149	-	134	58.1	27.03
9	PCD	149	-	133	58.4	24.97
10	PCAL1_0.0045	149	151	127	57.5	31.37
11	PCAL2_0.009	145	151	122	56.8	32.22
12	PCAL0.5_0.0023	148	151	125	57.7	31.10
13	PCDAL1_0.0045	147	149	128	57.4	31.66
14	PCDAL2_0.009	144	150	121	57.1	29.55
15	PCDAL0.5_0.0023	148	-	129	58	29.52

The increase in the degree of crystallinity (XC) for PLA/LA, with or without CNC and/or DCP, when compared to neat PLA, is attributed to the enhanced mobility of both unmodified and grafted chains within the amorphous fraction of PLA. The improved dispersion and interfacial adhesion of CNC throughout the matrix, as observed in Figure 5a, support the grafting hypothesis. This hypothesis is further substantiated by the presence of LA/($Sn(Oct)_2$/$P(C_6H_5)_3$) catalyst and the polymerization chain formation.

In samples where LA was incorporated with $Sn(Oct)_2$/$P(C_6H_5)_3$ along with PLA determination, an increase in the degree of crystallinity was observed, as demonstrated from PCAL0.5_0.0023 to PCAL2_0.0023, indicating a synergistic nucleation effect. This led to a noticeable weakening (fragile characteristic) of PLA, as illustrated in Figure 5b. A similar behavior was evident in PDAL2_0.009, PCAL2_0.009, and PCDAL2_0.009.

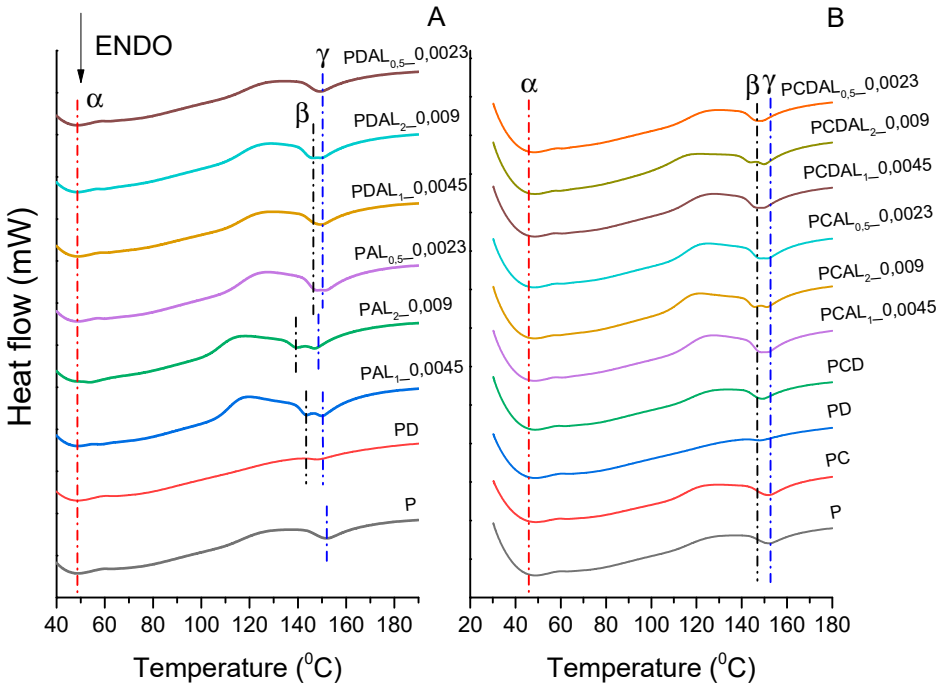

Preprints (www.preprints.org) | NOT PEER-REVIEWED | Posted: 17 November 2023 doi:10.20944/preprints202311.1154.v1

Figure 5. - DSC Curves for the Second Heating of Samples with Coupling Agents (DCP, LA, and $Sn(Oct)_2/P(C_6H_5)_3$) (b) DSC Curves for the Second Heating of Samples with Coupling Agents (DCP, LA, and $Sn(Oct)_2/P(C_6H_5)_3$) and CNC.

3.5. Mechanical characterization

Mechanical results and characterizations are presented in Figures 8 and 9, with values for Young's modulus and tensile strength shown in Table 4. Neat PLA specimens exhibited Young's modulus (E) ranging from 1.65 GPa and maximum tensile strength (σ_max) of 20.31 MPa. In the standard PC formulation, Young's modulus remained almost unchanged at 1.61 GPa, and the tensile strength was 18.93 MPa.

Additionally, the results for the standard PD formulation showed increases in both E and σ_max, by 46% to 54%, respectively, with average values of 2.54 GPa and 29.57 MPa, as demonstrated in Figure 6. Goffin A. L. et al. conducted a study on the increment of coercive force, attributing it to crosslink interactions in the reaction mechanism, resulting in macromolecule formation and enhanced nanocellulose crystallinity.

CNC and DCP were simultaneously introduced into the system (PCD) without causing changes in both Young's modulus (E) and maximum tensile strength (σ_max) when compared to neat PLA. In contrast, samples PDAL1_0.0045 and PDAL0.5_0.0023, where coupling agents DCP and LA up to 1.0 wt.% were associated with a catalyst system (Sn(Oct)2/P(C6H5)3), exhibited an approximate 50% increase in both E and σ_max. This supports the justification for the combined use of LA/ DCP catalyst. Additionally, this combination enhanced thermal properties, reducing thermal degradation, as confirmed by TGA. Samples PCAL1_0.0045 and PCAL0.5_0.0023, with an increment of 1 wt.% LA associated with a catalyst system ($Sn(Oct)_2/P(C_6H_5)_3$), CNC, and DCP, displayed an increase in both Young's modulus and tensile strength.

Furthermore, the improvement in mechanical properties can be attributed to the formation of crosslinking bonds, along with the presence of grafted structures such as PLA-g-CNC. This suggestion is supported by the FESEM micrographs shown in Figures 3d and 3e.

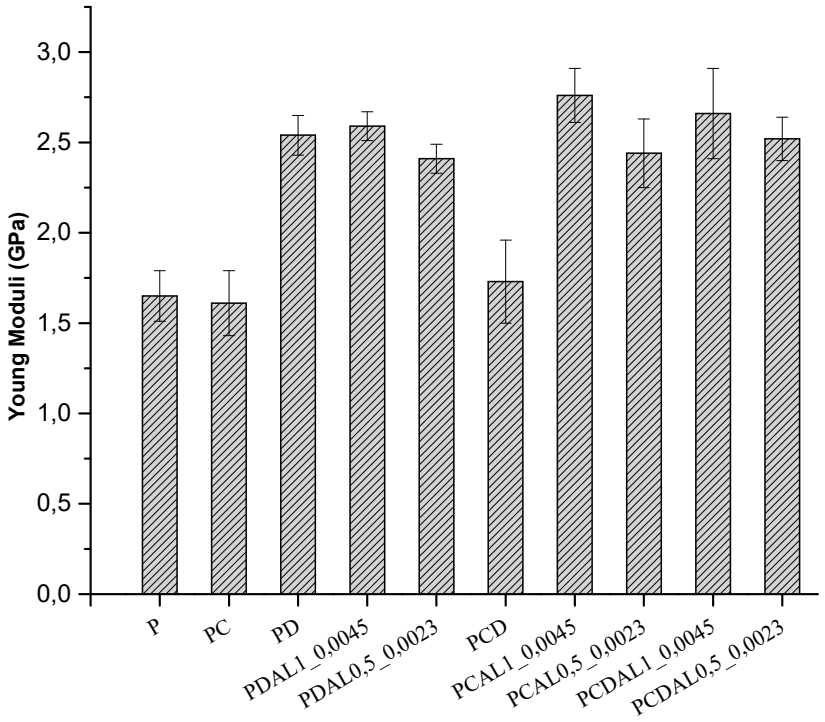

Figure 6. Young modulus of neat PLA and composites.

Preprints (www.preprints.org) | NOT PEER-REVIEWED | Posted: 17 November 2023 doi:10.20944/preprints202311.1154.v1

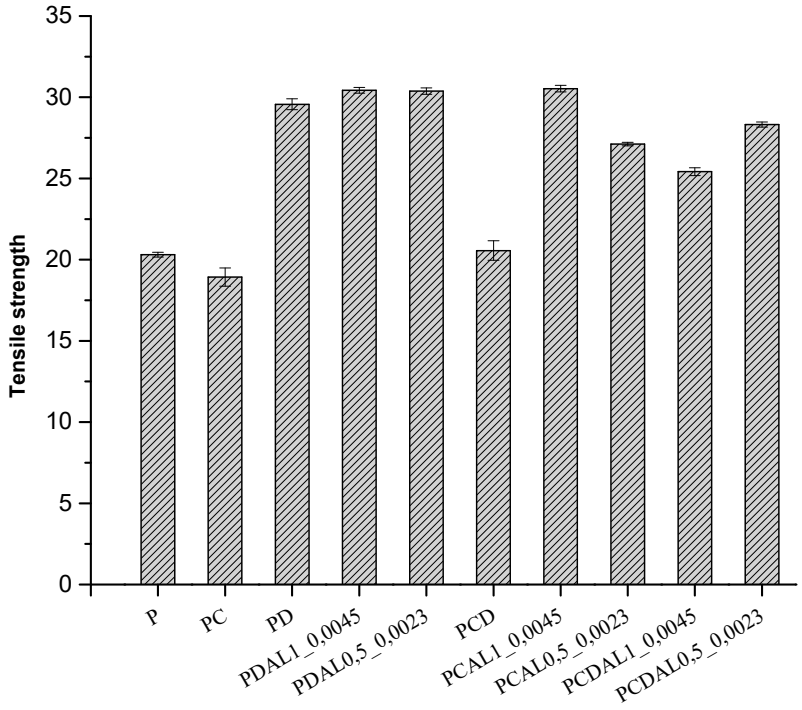

Figure 7. Tensile strength of neat PLA and composites.

4. Result and discursion

Reactive extrusion processing has been successfully applied to produce PLA-g-CNC composites. The material was processed with the addition of CNC and coupling agents DCP and LA in conjunction with $Sn(Oct)_2/P(C_6H_5)_3$. PLA/CNC grafting (PLA-g-CNC) was observed in FTIR analysis for samples with and without DCP and was confirmed by RNM analysis. DSC analyses showed that adding CNC to PLA increased the number of crystallites, resulting in better dispersion of CNC throughout the matrix. Increases in thermal stability were also observed for some contents of CNC and coupling agents, as confirmed by thermal results from TGA. Mechanical analyses suggested improvements in material properties, such as Young's modulus and tensile strength. In general, morphological analysis of failure surfaces showed good matrix-fiber interaction, indicating improvements in interfacial adhesion. Overall, this approach showed that reactive extrusion processing is a promising method for producing PLA-g-CNC biodegradable composites.

Author Contributions: For research articles with several authors, a short paragraph specifying their individual contributions must be provided. The following statements should be used João J. Melo dos Santos: Methodology, wrote – original draft investigation and Data acurration. Evanimek B. sabino da Silva: Methodology, Data acurration, Wrote – Original draft, and Investigation. Carlos A. Paskocimas: Financial support. Please turn to the CRediT taxonomy for the term explanation. Authorship must be limited to those who have contributed substantially to the work reported.

Funding: Please add: General financial support received from CAPES. No interference with study design and data analysis.Program code 23001011012P3, process 88887.465236/2019-00 for his fellowship.

Data Availability Statement: Not applicable.

Acknowledgments: All authors are grateful for the financial support of the Coordenação de Aperfeiçoamento de Pessoal de Nível Superior (CAPES) - Finance Code 001. E. B. Sabino da Silva thanks to the Universidade Federal do Rio Grande do Norte (UFRN) and Programa Nacional de pós - doutoramento (PNPD-CAPES), program code 23001011012P3, process 88887.465236/2019-00 for his fellowship.

Conflicts of Interest: The authors declare no conflict of interest.

References

1. Vatansever, E.; Arslan, D.;; Nofar, M. Polylactide Cellulose-Based Nanocomposites. *Int J Biol Macromol* **2019**, *137*, 912–938.
2. Laycock, B.; Nikolić, M.; Colwell, J.M.; Gauthier, E.; Halley, P.; Bottle, S.; George, G. Lifetime Prediction of Biodegradable Polymers. *Prog Polym Sci* **2017**, *71*, 144–189, doi:10.1016/j.progpolymsci.2017.02.004.
3. A-Review-on-the-Polymeric-Laminates-Reinforced-with-Natural-FibersJournal-of-Reinforced-Plastics-and-Composites.Pdf.
4. Dhar, P.; Tarafder, D.; Kumar, A.; Katiyar, V. Thermally Recyclable Polylactic Acid/Cellulose Nanocrystal Films through Reactive Extrusion Process. *Polymer (United Kingdom)* **2016**, *87*, 268–282, doi:10.1016/j.polymer.2016.02.004.
5. Sypaseuth, F.D.; Gallo, E.; Çiftci, S.; Schartel, B. Polylactic Acid Biocomposites: Approaches to a Completely Green Flame Retarded Polymer. *E-Polymers* **2017**, *17*, 449–462, doi:10.1515/epoly-2017-0024.
6. Zhou, Y.; Katsou, E.; Fan, M. International Journal of Biological Macromolecules Interfacial Structure and Property of Eco-Friendly Carboxymethyl Cellulose / Poly (3-Hydroxybutyrate- Co -3-Hydroxyvalerate) Biocomposites. *Int J Biol Macromol* **2021**, *179*, 550–556, doi:10.1016/j.ijbiomac.2021.03.009.
7. Dickmann, M.; Tarter, S.; Egger, W.; Pegoretti, A.; Rigotti, D.; Brusa, R.S. Interface Nanocavities in Poly (Lactic Acid) Membranes with Dispersed Cellulose Nanofibrils : Their Role in the Gas Barrier Performances. *Polymer (Guildf)* **2020**, *202*, 122729, doi:10.1016/j.polymer.2020.122729.
8. Cheong, W.J.; Yang, S.H.; Ali, F. Molecular Imprinted Polymers for Separation Science: A Review of Reviews. *J Sep Sci* **2013**, *36*, 609–628, doi:10.1002/jssc.201200784.
9. Kumar, A.; Dutta, S.; Kwon, S.; Kwon, T.; Patil, S.S.; Kumari, N.; Jeevanandham, S.; Lee, I.S. Solid-State Reaction Synthesis of Nanoscale Materials: Strategies and Applications. *Chem Rev* **2022**, doi:10.1021/acs.chemrev.1c00637.
10. Francavilla, M.; Pineda, A.; Lin, C.S.K.; Franchi, M.; Trotta, P.; Romero, A.A.; Luque, R. Natural Porous Agar Materials from Macroalgae. *Carbohydr Polym* **2013**, *92*, 1555–1560, doi:10.1016/j.carbpol.2012.11.005.
11. Lima, L.R.; Santos, D.B.; Santos, M.V.; Barud, H.S.; Henrique, M.A.; Pasquini, D.; Pecoraro, E.; Ribeiro, S.J.L. Cellulose Nanocrystals from Bacterial Cellulose | Nanocristais de Celulose a Partir de Celulose Bacteriana. *Quim Nova* **2015**, *38*, 1140–1147, doi:10.5935/0100-4042.20150131.
12. De Jesus Silva, D.; D'Almeida, M.L.O. *O Papel (Brazil)*. 2009, pp. 34–52.
13. Gutiérrez, M.C.; Rosa, P.T.V.; De Paoli, M.-A.; Felisberti, M.I. Biocomposites Based on Cellulose Acetate and Short Curaua Fibers Treated with Supercritical CO<inf>2</Inf> | Biocompósitos de Acetato de Celulose e Fibras Curtas de Curauá Tratadas Com CO<inf>2</Inf> Supercrítico. *Polimeros* **2012**, *22*, 295–302, doi:10.1590/S0104-14282012005000037.
14. Carvalho, A. *O Papel (Brazil)*. 2008, pp. 36–41.
15. Dhar, P.; Tarafder, D.; Kumar, A.; Katiyar, V. Effect of Cellulose Nanocrystal Polymorphs on Mechanical, Barrier and Thermal Properties of Poly(Lactic Acid) Based Bionanocomposites. *RSC Adv* **2015**, *5*, 60426–60440, doi:10.1039/c5ra06840a.
16. Dhar, P.; Gaur, S.S.; Soundararajan, N.; Gupta, A.; Bhasney, S.M.; Milli, M.; Kumar, A.; Katiyar, V. Reactive Extrusion of Polylactic Acid/Cellulose Nanocrystal Films for Food Packaging Applications: Influence of Filler Type on Thermomechanical, Rheological, and Barrier Properties. *Ind Eng Chem Res* **2017**, *56*, 4718–4735, doi:10.1021/acs.iecr.6b04699.
17. Bitinis, N.; Fortunati, E.; Verdejo, R.; Bras, J.; Kenny, J.M.; Torre, L.; López-Manchado, M.A. Poly(Lactic Acid)/Natural Rubber/Cellulose Nanocrystal Bionanocomposites. Part II: Properties Evaluation. *Carbohydr Polym* **2013**, *96*, 621–627, doi:10.1016/j.carbpol.2013.03.091.
18. Shehzad, Q.; Liu, Z.; Zuo, M.; Wang, J. The Role of Polysaccharides in Improving the Functionality of Zein Coated Nanocarriers: Implications for Colloidal Stability under Environmental Stresses. *Food Chem* **2024**, *431*, doi:10.1016/j.foodchem.2023.136967.
19. Bhat, M.I.; Shahi, N.C.; Lohani, U.C.; Pathania, S.; Malik, S.; Singh, S.; Amin, T. Cellulose Nanocrystals Reinforced Chitosan/Titanium Dioxide Bionanocomposite with Enhanced Interfacial Compatibility: Fabrication, Characterization, and Application in Fresh-Cut Apple Slices. *Int J Biol Macromol* **2023**, *253*, doi:10.1016/j.ijbiomac.2023.127498.
20. Karamanlioglu, M.; Preziosi, R.; Robson, G.D. Abiotic and Biotic Environmental Degradation of the Bioplastic Polymer Poly(Lactic Acid): A Review. *Polym Degrad Stab* **2017**, *137*, 122–130.
21. Dufresne, A. Cellulose Nanomaterial Reinforced Polymer Nanocomposites. *Curr Opin Colloid Interface Sci* **2017**, *29*, 1–8, doi:10.1016/j.cocis.2017.01.004.
22. Karamanlioglu, M.; Yesilkir-Baydar, S. Characterization of Gelatin-Based Wound Dressing Biomaterials Containing Increasing Coconut Oil Concentrations. *J Biomater Sci Polym Ed* **2023**, doi:10.1080/09205063.2023.2265624.
23. Salmieri, S.; Islam, F.; Khan, R.A.; Hossain, F.M.; Ibrahim, H.M.M.; Miao, C.; Hamad, W.Y.; Lacroix, M. Antimicrobial Nanocomposite Films Made of Poly(Lactic Acid)-Cellulose Nanocrystals (PLA-CNC) in

Food Applications: Part A-Effect of Nisin Release on the Inactivation of Listeria Monocytogenes in Ham. *Cellulose* **2014**, *21*, 1837–1850, doi:10.1007/s10570-014-0230-6.
24. Kargarzadeh, H.; Mariano, M.; Huang, J.; Lin, N.; Ahmad, I.; Dufresne, A.; Thomas, S. Recent Developments on Nanocellulose Reinforced Polymer Nanocomposites: A Review. *Polymer (United Kingdom)* **2017**, *132*, 368–393, doi:10.1016/j.polymer.2017.09.043.
25. Dhar, P.; Bhasney, S.M.; Kumar, A.; Katiyar, Vimal. *POLYMER*. 2016, pp. 75–92.
26. Shah, A.A.; Hasan, F.; Hameed, A.; Ahmed, S. Biological Degradation of Plastics: A Comprehensive Review. *Biotechnol Adv* **2008**, *26*, 246–265, doi:10.1016/j.biotechadv.2007.12.005.
27. Murariu, M.; Dubois, P. PLA Composites: From Production to Properties. *Adv Drug Deliv Rev* **2016**, *107*, 17–46, doi:10.1016/j.addr.2016.04.003.
28. Niaounakis, M. *Biopolymers - Applications and Trends*; 2015; ISBN 9780323266987.
29. Hartmann, M.H. High Molecular Weight Polylactic Acid Polymers BT - Biopolymers from Renewable Resources. **1998**, 367–411, doi:10.1007/978-3-662-03680-8_15.
30. Jeziórska, R. Effects of Bis(2-Oxazoline) Derivative as Compatibilizer and Reactive Extrusion Conditions on the Properties of Polyamide 6 / Poly(Ethylene Terephthalate) Blends | Wpływ Pochodnej Bis(2-Oksazoliny) Jako Kompatybilizatora Oraz Warunków Wytłaczania Reaktywn. *Polimery/Polymers* **2006**, *51*, 351–358, doi:10.14314/polimery.2006.351.
31. Mignon, A.; De Belie, N.; Dubruel, P.; Van Vlierberghe, S. Superabsorbent Polymers: A Review on the Characteristics and Applications of Synthetic, Polysaccharide-Based, Semi-Synthetic and 'Smart' Derivatives. *Eur Polym J* **2019**, *117*, 165–178, doi:10.1016/j.eurpolymj.2019.04.054.
32. Hatti-Kaul, R.; Nilsson, L.J.; Zhang, B.; Rehnberg, N.;; Lundmark, S. Review - Designing Biobased Recyclable Polymers for Plastics. *Trends Biotechnol* **2019**, 1–18.
33. Kalia, S.; Dufresne, A.; Cherian, B.M.; Kaith, B.S.; Avérous, L.; Njuguna, J.; Nassiopoulos, E. Cellulose-Based Bio- and Nanocomposites: A Review. *Int J Polym Sci* **2011**, 1–35, doi:10.1155/2011/837875.
34. Suryanarayana, C.; Al-Aqeeli, N. Mechanically Alloyed Nanocomposites. *Prog Mater Sci* **2013**, *58*, 383–502, doi:10.1016/j.pmatsci.2012.10.001.
35. Ahmad, E.E.M.; Luyt, A.S. Morphology, Thermal, and Dynamic Mechanical Properties of Poly(Lactic Acid)/Sisal Whisker Nanocomposites. *Polym Compos* **2012**, *33*, 1025–1032, doi:10.1002/pc.22236.
36. Muñoz, P.A.R.; Bettini, S.H.P. Assessment of the Utilization of Different Peroxide Dispersion Media on the Controlled Degradation of Polypropylene. *Journal of Applied Polymer Science* **2013**, *127*, 87–95, doi:10.1002/app.36705.
37. Jacobsen, S.; Fritz, H.G.; Degée, P.; Dubois, P.; Jérôme, R. New Developments on the Ring Opening Polymerisation of Polylactide. *Ind Crops Prod* **2000**, *11*, 265–275, doi:10.1016/S0926-6690(99)00053-9.
38. Raquez, J.M.; Narayan, R.; Dubois, P. Recent Advances in Reactive Extrusion Processing of Biodegradable Polymer-Based Compositions. *Macromolecular Materials and Engineering* **2008**, *293*, 447–470, doi:10.1002/mame.200700395.
39. Ahmad, E.E.M.; Luyt, A.S. Morphology , Thermal , and Dynamic Mechanical Properties of Poly (Lactic Acid)/ Sisal Whisker Nanocomposites. *Polym Compos* **2012**, *33*, 1025–1032, doi:10.1002/pc.
40. Dhar, P.; Tarafder, D.; Kumar, A.; Katiyar, V. Thermally Recyclable Polylactic Acid/Cellulose Nanocrystal Films through Reactive Extrusion Process. *Polymer (Guildf)* **2016**, *87*, 268–282, doi:10.1016/j.polymer.2016.02.004.